Real-time dissociation dynamics of the Ne_2Br_2 van der Waals complex

Jordan M. Pio, Molly A. Taylor, Wytze E. van der Veer, Craig R. Bieler,[a] Jose A. Cabrera,[b] and Kenneth C. Janda[c]

Department of Chemistry and Institute of Surface and Interface Science, University of California, Irvine, California, 92697-2025, USA

(Received 28 April 2010; accepted 1 June 2010; published online 7 July 2010)

We have characterized the vibrational predissociation (VP) of the Ne_2Br_2 van der Waals complex using time- and frequency-resolved pump-probe spectroscopy. After exciting Br_2 within the complex to a vibrational level $16 \leq \nu' \leq 23$ in the B state, we follow the flow of halogen vibrational energy to the van der Waals modes in real time by recording the time-dependent behavior of Ne_2Br_2 (ν'), the $NeBr_2$ $(\nu'-m)$ intermediates, and the Br_2 $(\nu'-n)$ products. For Ne_2Br_2 $(\nu'=16-18)$, the only intermediate observed is $NeBr_2$ $(\nu'-1)$, and the majority of the final product is Br_2 $(\nu'-2)$, indicating the dissociation happens via two sequential direct VP steps. We fit the time-dependent behavior of these species to a sequential mechanism and extracted time constants for each step. For higher ν' levels, the results show that the dissociation occurs via multiple pathways. Product Br_2 from levels lower than $(\nu'-2)$ becomes much more important, with products as low as $(\nu'-5)$ being observed. For $\nu'=21$, we observe both $NeBr_2$ $(\nu'-1)$ and $(\nu'-2)$ intermediates. The intermediates have significantly different kinetics, with the decay rate of the $(\nu'-1)$ transient being nearly twice that of the $(\nu'-2)$ transient. Similarly, both Br_2 $(\nu'-2)$ and $(\nu'-3)$ are formed in almost equal amounts, but the $(\nu'-2)$ product formation rate is faster than the $(\nu'-3)$ rate. The broad vibrational product state distributions and multiple dissociation pathways indicate that intramolecular vibrational energy redistribution becomes increasingly important for $\nu'>19$. We also report vibrational product state distributions for direct excitation to $NeBr_2$ $16 \leq \nu' \leq 23$. For $NeBr_2$, the dominant product channel is Br_2 $(\nu'-1)$ for all initial ν' studied, consistent with this complex dissociating primarily via direct VP. © *2010 American Institute of Physics*.
[doi:10.1063/1.3456550]

I. INTRODUCTION

One of the major motivations for research on weakly bound gas phase clusters is to better understand the transition from the gas to condensed phase. These studies are often performed by embedding a chromophore in a size-selected cluster and following the photodynamics as the number of solvent species is increased. Usually charged species are studied because they are easily size-selected with mass spectrometry. For example, Lineberger and co-workers[1,2] studied the geminate recombination of I_2^- (and other halogen anions) embedded in a cluster of CO_2 molecules after excitation of I_2^- to repulsive electronic states. Even with only a few CO_2 solvent molecules present, solvent caging effects are observed. Similar studies on the size dependence of dynamics in neutral clusters are much more challenging because of the technical difficulties in studying neutral clusters with a well-defined number of solvent species attached to the chromophore.

In this regard, neutral clusters consisting of a diatomic halogen (X_2) with one or more rare gas (Rg) atoms attached have a number of advantages. They can be size-selected spectroscopically, as the addition of each rare atom induces a blueshift in the halogen $(B,\nu') \leftarrow (X,\nu''=0)$ vibronic transition.[3,4] Despite their apparent simplicity, these rare gas–halogen complexes (Rg_NX_2) undergo a variety of photodissociation dynamics after excitation of the halogen, even for the $N=1$ clusters.[5] In the process called vibrational predissociation (VP), the $RgX_2(B,\nu')$ complex fragments due to the transfer of halogen vibrational energy to the van der Waals bond: $RgX_2(B,\nu') \rightarrow Rg+X_2(B,\nu'-n)$. When one quantum of X_2 vibrational energy is sufficient to dissociate the Rg atom, direct VP preferentially occurs. In direct VP, the quasibound RgX_2 (B,ν') state couples directly to the $Rg+X_2$ $(B,\nu'-1)$ continuum, and the predissociation rate is described by Fermi's golden rule.[6,7] As one excites to higher X_2 stretching levels, the individual vibrational quanta become smaller and the $\Delta\nu'=-1$ channel gradually closes, beginning with a decreasing number of $X_2(\nu'-1)$ rotational levels available as product states. As this closing occurs, the dissociation mechanism switches to intramolecular vibrational energy redistribution (IVR), in which the initial quasibound state accesses the $\Delta\nu'=-2$ product states via "doorway" $(\nu'-1)$ excited van der Waals levels.[8,9] The Rg atom can also induce electronic predissociation (EP) by coupling the halogen B electronic state to repulsive states, breaking the halogen bond, and forming free halogen atoms.[10,11]

While many rare gas–halogen complexes with more than one Rg atom attached have been observed via the halogen $B \leftarrow X$ transition,[3,4,12–18] there is little detailed experimental

[a]Present address: Chemistry Department, Albion College, Albion, Michigan.
[b]Present address: San José City College, San José, California.
[c]Electronic mail: kcjanda@uci.edu.

data on the dissociation dynamics of these larger complexes after excitation to the B state, especially compared to the very well-characterized dissociation dynamics of the RgX_2 complexes. The primary experimental results on the dissociation dynamics of Rg_NX_2 (ν') complexes are the final product state distributions of the X_2 $(\nu'-n)$. Both He_NI_2 $(\nu'=20-21)$ (Ref. 3) and He_NCl_2 $(\nu'=8)$ (Refs. 13 and 19–21) dissociate primarily into X_2 $(\nu'-N)$. The dissociation of each He atom takes one quantum of vibrational energy even though energetically one quantum of Cl_2 or I_2 stretching vibration could dissociate many He atoms. From these results, it was concluded that each He atom is dynamically independent; they interact so weakly that energy is not shared between them. Therefore, the He complexes dissociate through a series of sequential direct VP steps. The halogen vibrational energy is lost one quantum at a time. Each quantum of energy goes to a single He-X_2 bond so that only one He atom is dissociated for each quantum transferred.

The size dependence of the Ne_NI_2 $(\nu'=20-21)$ (Ref. 4) and Ne_NCl_2 $(\nu'=7-13)$ (Refs. 14 and 22) vibrational product state distributions is qualitatively different from that of the He complexes. Like the He complexes, the $N=1$ neon complexes undergo direct VP and form primarily X_2 $(\nu'-1)$. However, the predissociation of the larger clusters does not appear to follow the sequential direct VP mechanism, as other product channels besides $(\nu'-N)$ are significant. For Ne_2Cl_2 $(\nu'<9)$, significant Cl_2 $(\nu'-1)$ product is formed, indicating that vibrational energy can be shared between the two Ne stretching degrees of freedom. Ne_2I_2 $(\nu'=21)$ also does not dissociate via sequential direct VP, as nearly equal amounts of I_2 $(\nu'-2)$ and $(\nu'-3)$ are formed. The appearance of the $(\nu'-3)$ product may result from some of the vibrational energy being transferred to nondissociative van der Waals modes so that the loss of one stretch quantum to the Ne degrees of freedom does not necessarily lead to the loss of one Ne atom. The product vibrational distributions for the Ne_NX_2 (ν') complexes indicate the increasing complexity of the vibrational energy transfer mechanisms from the halogen "solute" to the rare gas "solvent," with the additional Ne–Ne degrees of freedom altering the dynamics from the sequential direct dissociation mechanism. In this sense, Ne is a "stronger solvent" than He.

The more complicated dissociation mechanisms with increasing cluster size make detailed characterization of the energy transfer much more difficult. Experimentally, the primary challenge is in identifying the various intermediate species that are generated as a consequence of the energy flow. Most of the experiments to date have been frequency domain studies. These experiments can measure the decay rate of the initially excited Rg_NX_2 (ν') from the homogeneous linewidth and record the final product state distributions. However, the intermediate steps of the dissociation cannot easily be observed in the frequency domain. Time-resolved experiments capable of recording the dynamics of all the species formed in the predissociation process are needed to study the larger complexes with more complicated dissociation mechanisms. Gutmann *et al.*[23] performed picosecond pump-probe experiments on Ne_2I_2 $(B,\nu'=17-23)$. However, they only recorded the formation of the final I_2 $(\nu'-n)$ products, not any intermediates. In order to infer the behavior of the intermediates, they fitted the final product I_2 formation traces to an assumed sequential first order kinetic mechanism.

The larger rare gas–halogen complexes provide significant challenges for theory as well. For the triatomic complexes, exact full-dimensional quantum calculations of the VP dynamics are feasible, with the accuracy limited by the assumed potential energy surface. Impressive agreement has been achieved between experimentally measured and theoretically calculated state-to-state dynamics of the RgX_2 complexes.[19] However, for the larger complexes, the rapidly increasing number of degrees of freedom make full-dimensional quantum calculations difficult, if not impossible. The vast majority of theoretical studies on Rg_NX_2 $(N>1)$ dissociation[20,21,24–45] have used various approximate methods (reduced-dimensionality quantum calculations and classical or mixed quantum-classical methods, for instance), with only a handful of exact full-dimensional quantum calculations being performed for $N=2$ complexes.[26,45] The dissociation of the larger Rg_NX_2 clusters provides an important test for development of approximate methods that can accurately describe the dynamics with reasonable computational effort. Thus, more detailed experimental data are needed for comparison. In particular, direct observation of intermediate steps along the dissociation path will be very valuable.

Recently, we have used time- and frequency-resolved pump-probe spectroscopy to study the dissociation dynamics of $HeBr_2$, $NeBr_2$, and $ArBr_2$.[11,46–48] With the 35 ps time resolution of our pump-probe setup, we have been able to record the time-dependent behavior of both the decay of the initial Rg-Br_2 and the formation of the Br_2 product. In this paper, we have extended this line of work to record the transient species in the dissociation of the Ne_2Br_2 complex, measuring directly the decay of the initially prepared Ne_2Br_2 (B,ν'), the formation and decay of the intermediates $NeBr_2$ $(B,\nu'-m)$, and the formation of the product Br_2 $(B,\nu'-n)$. Thus, we are able to study the complicated multistep dissociation of the Rg_2X_2 clusters at a level of detail not achieved in previous experiments.

II. EXPERIMENTAL

The Ne_2Br_2 complexes are studied using an experimental apparatus and methods similar to those used in our time-resolved pump-probe spectroscopy on $He^{79}Br_2$,[11] $Ne^{79}Br_2$,[11,46] and $Ar^{79}Br_2$ (Ref. 47) dissociation dynamics. The pump-probe scheme used for studying Ne_2Br_2 is shown in Fig. 1. The pump laser is tuned to excite the Br_2 within the complex from the $(X,\nu''=0)$ ground vibronic state of Br_2 to a chosen (B,ν') state. Because the Ne–Br_2 interaction minimally perturbs the electronic structure of Br_2, for convenience the state of the complex prepared by the laser is denoted by the dominant character of the Br_2 within the complex, for example, Ne_2Br_2 (B,ν'). After excitation, the Ne_2Br_2 (B,ν') undergoes VP, dissociating the Ne atoms to form the Br_2 $(B,\nu'-n)$ products and possibly $NeBr_2$ $(B,\nu'-m)$ intermediates. All these species formed in the VP process are detected by exciting with the probe pulse the Br_2

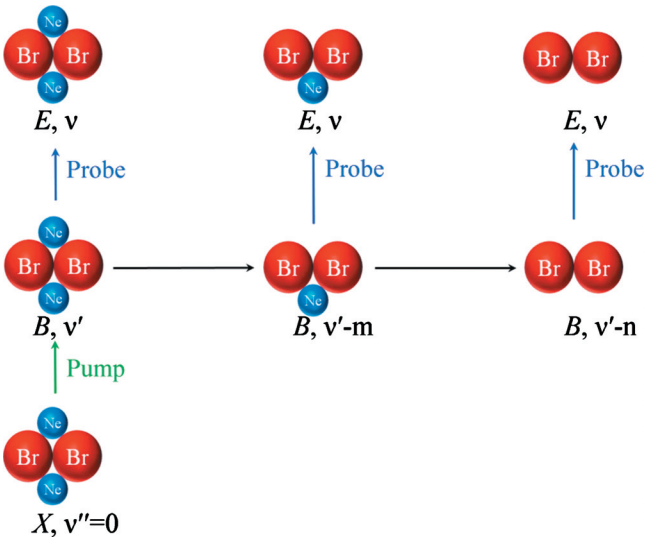

FIG. 1. Pump-probe scheme used to characterize the Ne_2Br_2 predissociation dynamics.

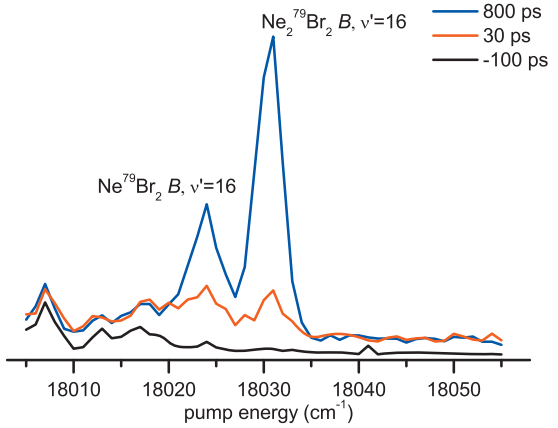

FIG. 2. Excitation spectra over the $B \leftarrow X$, $16 \leftarrow 0$ region obtained with the probe laser fixed on the Br_2 $E \leftarrow B$, $1 \leftarrow 14$ transition. The spectra were taken with the probe delayed relative to the pump by −100 ps (black), 30 ps (red), and 800 ps (blue).

(either free or within the complex of interest) to a vibrational level ν in the E electronic state and recording the resulting fluorescence.

We perform three types of experiments, depending on whether the pump energy, probe energy, or pump-probe time delay is being varied. To identify the $B \leftarrow X$, $\nu' \leftarrow \nu''=0$ pump transitions of the Ne_2Br_2 complex, we perform excitation scans, where the wavelength of the pump pulse is scanned while the probe pulse is fixed on a free Br_2 $E \leftarrow B$, $\nu \leftarrow \nu'$ transition.[49] Once the pump transitions are found, we perform probe scans with the pump pulse fixed to excite the Ne_2Br_2 (B,ν') complex. From these probe scans, we find the $E \leftarrow B$ probe transitions of the initially prepared Ne_2Br_2 (B,ν'), intermediate $NeBr_2$ $(B,\nu'-m)$, and product Br_2 $(B,\nu'-n)$. Finally, we record the time-dependent behavior of all the species that are formed in the Ne_2Br_2 (B,ν') predissociation by fixing the probe on the corresponding $E \leftarrow B$ transition and scanning the time delay between the pump and the probe pulses.

The complexes are formed by first passing a 50% He/50% Ne gas mixture at ≈12.5 bars over solid Br_2 held at −15 °C and then expanding the gas mixture into a vacuum chamber through a 150 μm diameter pulsed nozzle. The supersonic free jet expansion rapidly cools the gas mixture, leading to the formation of van der Waals complexes.

The pump and probe pulses are created from two independently tunable optical parametric oscillator-optical parametric amplifiers pumped by the third harmonic of a single mode-locked neodymium:yttrium aluminum garnet laser.[50] The pulses have spectral and temporal widths of about 2 cm^{-1} and 35 ps (full width at half maximum). The pump and probe pulses are combined on a dichroic mirror and pass collinearly into the vacuum chamber, intersecting the free jet expansion at a right angle 2.0–3.0 cm downstream from the nozzle. The time delay between the pump and the probe pulses is controlled by changing the path length of the pump laser with a delay stage. Fluorescence from the E state is recorded using a photomultiplier tube (PMT). The pump and probe pulses are linearly polarized, with the angle between the pump and probe polarizations controlled by passing the pump pulse through a broadband half-wave plate. Experiments were performed at multiple polarization orientations, and there was no observed effect of the polarization angle on the experimental results. Unless otherwise noted, all the results presented here are for the $^{79}Br_2$ isotopomer.

III. RESULTS

A. Excitation spectra

Figure 2 shows the excitation spectra obtained by scanning the pump laser over the $B \leftarrow X$, $\nu'=16 \leftarrow \nu''=0$ region while monitoring the E-state fluorescence with the probe laser fixed on the free Br_2 $E \leftarrow B$, $\nu=1 \leftarrow \nu'=14$ transition. Three spectra are shown, each at a different pump-probe delay. When the probe pulse arrives 800 ps after the pump pulse, the spectrum has two prominent features that are assigned to the $NeBr_2$ and Ne_2Br_2 $B \leftarrow X$, $16 \leftarrow 0$ transitions. The peaks are assigned using the band shift rule, where the addition of each Ne atom induces a 6–7 cm^{-1} blueshift in the Br_2 $B \leftarrow X$ transition.[17] The $NeBr_2$ transition at 18024 cm^{-1} is 6 cm^{-1} to the blue of the free Br_2 $B \leftarrow X$, $16 \leftarrow 0$ transition. The addition of a second Ne atom causes a further 6–7 cm^{-1} blueshift, and so the peak at 18031 cm^{-1} is assigned to the Ne_2Br_2 transition. These transitions are observed because both complexes can predissociate to form the product free Br_2 $(B,\nu'=14)$ detected by the probe laser. When the probe pulse arrives 100 ps before the pump pulse (denoted as −100 ps), the Ne_NBr_2 transitions are not observed since the complexes have not yet been excited. When the probe is delayed 30 ps relative to the pump, the complexes have had little time to predissociate and form the product, so the transitions of the complexes are weak compared to those obtained at the 800 ps time delay.

The 2 cm^{-1} bandwidth of the pump pulse is too broad to observe any rotational features in the vibronic transitions, making it impossible to establish the structure of the Ne_NBr_2 complexes or measure the rotational temperature of the free jet. However, on the basis of previous works,[14,51] the likely

structures of the $NeBr_2$ and Ne_2Br_2 complexes excited in the spectra of Fig. 2 are those with the Ne atom(s) attached perpendicular to the Br–Br bond. This $NeBr_2$ T-shaped structure has been confirmed directly by Thommen *et al.* by fitting the high resolution spectrum of the $NeBr_2$ $B \leftarrow X$, 10 $\leftarrow 0$ band.[51] No such high resolution spectrum has been obtained for Ne_2Br_2. However, the fact that the blueshift is the same when adding the second Ne atom implies that this atom occupies an equivalent location as the first Ne atom so that the probable structure of the Ne_2Br_2 complex is a distorted tetrahedron, with both Ne atoms perpendicular to the Br–Br bond. This distorted tetrahedral geometry has been confirmed experimentally from fits to the rotational structure of the analogous Ne_2Cl_2 $B \leftarrow X$ bands.[14]

Any structure in which one of the Ne atoms was located on the end of the Br_2 would be excited to the repulsive wall of the intermolecular continuum that asymptotically correlates with free Br_2 $v'=14$, leading to excitation bands much broader than the two peaks observed in Fig. 2. In fact, this broad continuum does underlie the two peaks in Fig. 2, leading to an apparent increase of the baseline in the spectrum measured at a 30 ps delay. Because the discrete transitions of the perpendicular Ne_NBr_2 complexes sit on top of this background, the time-dependent behavior of the linear isomer dissociation must be taken into account in the analysis of the delay scans. See Ref. 48 for details on the spectra of the linear isomers.

The excitation of the perpendicular Ne_NBr_2 complexes leaves the van der Waals modes in the ground state. This is because the minimum of the B-state van der Waals potential is only slightly displaced from the X-state van der Waals minimum.[52] So, Franck–Condon factors strongly favor transitions from the lowest van der Waals level of the X state to the lowest van der Waals level of the B state. Direct excitation to excited van der Waals levels has been observed,[48,53,54] but such transitions in the Ne_NBr_2 complexes would be further to the blue of the peaks in Fig. 2.

The peaks on the low energy side of the spectra in Fig. 2 are due to a small amount of $B \rightarrow X$ fluorescence of free Br_2 leaking through the UG-5 colored glass filter in front of the PMT. Because the fluorescence is from the B state, it is independent of the pump-probe delay.

Figure 3 shows excitation spectra obtained by tuning the pump over the $B \leftarrow X$, $17 \leftarrow 0$ region with the probe laser fixed on the $NeBr_2$ $E \leftarrow B$, $2 \leftarrow 16$ transition at three different pump-probe delays. (The assignment of the probe transitions of the complex is described in Sec. III B.) When the probe arrives 30 ps after the pump, a peak due to Ne_2Br_2 $(B, v'=17)$ is present, indicating that after 30 ps a significant fraction of Ne_2Br_2 $(B, v'=17)$ has decayed into the $NeBr_2$ $(B, v'=16)$ complex detected by the probe laser. There is also a $Ne_2{}^{79-81}Br_2$ peak due to overlapping probe transitions. At an 800 ps pump-probe delay, the Ne_2Br_2 $(B, v'=17)$ peak has disappeared due to the decay of the $NeBr_2$ $(B, v'=16)$ intermediate. One puzzling feature of these scans is the background signal that is present at 30 ps but disappears at long delay times. While the linear isomer might seem to be the most likely source of this transient continuum, the background decays with a single exponential time constant between 50 and 100 ps, too slow for the ultrafast direct dissociation of the linear isomer. One possibility is that the transient background originates from the excitation of a "police nightstick" Ne_2Br_2 isomer, with one Ne atom in the T-shaped position and the other in the linear position.[16] The isomer would have a broad spectrum from the Ne atom in the linear position, and after excitation would rapidly dissociate to form T-shaped $NeBr_2$. The slow decay of the background is consistent with the predissociation of these T-shaped $NeBr_2$ (B, v') complexes. As with the linear isomer contribution, this time-dependent background must be accounted for when recording the time-dependent behavior of the Ne_2Br_2 complex.

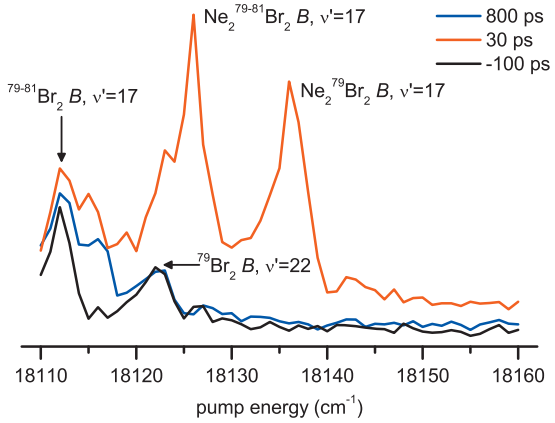

FIG. 3. Excitation spectra over the $B \leftarrow X$, $17 \leftarrow 0$ region obtained with the probe laser fixed on the $NeBr_2$ $E \leftarrow B$, $2 \leftarrow 16$ transitions. The spectra were taken with the probe delayed relative to the pump by -100 ps (black), 30 ps (red), and 800 ps (blue).

B. Probe spectra

1. $NeBr_2$ *probe spectra*

After the $B \leftarrow X$ transitions of the complexes are identified, probe spectra are obtained to identify the $E \leftarrow B$, $v \leftarrow v'$ probe transitions of the $NeBr_2$ and Ne_2Br_2 complexes. Making these assignments is crucial because to fully characterize the predissociation of Ne_2Br_2, we must characterize the intermediate species formed in the predissociation process.

The $NeBr_2$ $E \leftarrow B$, $v \leftarrow v'$ transitions are assigned from probe spectra recorded with the pump laser tuned to directly excite $NeBr_2$ (B, v').[46] Figure 4(a) shows probe spectra recorded after exciting to $NeBr_2$ $(B, v'=21)$. When the probe arrives 800 ps after the pump, the initially prepared $NeBr_2$ $v'=21$ has dissociated, and the major peaks are the probe transitions of the product Br_2 $v'=19$ and 20. Consistent with the direct VP mechanism, the $(v'-1)$ product channel is dominant. The very weak transitions that can be seen on the shoulders of the main peaks and around 32 060 cm^{-1} are products of the direct dissociation of the linear isomer, which has a very broad Br_2 vibrational product state distribution.[48] When the pump-probe delay is 10 ps, the probe spectrum contains two prominent peaks at 32 057 and 32 200 cm^{-1} that are not present at 800 ps delay. This indicates that they are due to the decaying $NeBr_2$ species. These peaks are assigned to be $NeBr_2$ $E \leftarrow B$, $6 \leftarrow 21$ and $7 \leftarrow 21$ transitions.

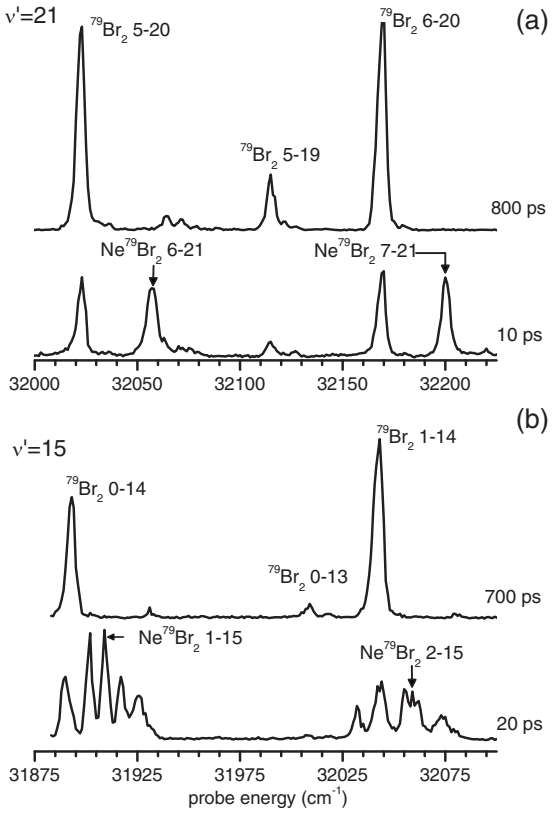

FIG. 4. Probe spectra recorded with the pump pulse fixed to excite (a) $NeBr_2$ $(B,\nu'=21)$ and (b) $NeBr_2$ $(B,\nu'=15)$. The labels on the peaks denote the $E \leftarrow B$, $\nu \leftarrow \nu'$ vibronic transitions. Each spectrum is labeled on the right according to the time delay of the probe relative to the pump.

The assignment is based on a band shift rule similar to the one used for the $B \leftarrow X$ transitions, with the addition of the Ne atom redshifting the transitions by 25 cm^{-1} from the corresponding free Br_2 transitions. Hair *et al.* observed a similar redshift in $NeCl_2$, with the $E \leftarrow B$, $0 \leftarrow 7$ transition redshifted by ≈ 20 cm^{-1} from the free Cl_2 transition.[14]

Unfortunately, the assignment of $NeBr_2$ $E \leftarrow B$ probe transitions was not always as straightforward as described in the previous paragraph. Figure 4(b) shows both short and long delay time probe spectra obtained after exciting to $NeBr_2$ $\nu'=15$. Compared to the short delay time probe spectrum for $\nu'=21$, the spectrum for $\nu'=15$ contains many transient features besides the $NeBr_2$ $E \leftarrow B$, $1 \leftarrow 15$ and $2 \leftarrow 15$ transitions that are assigned based on their redshift from the free Br_2 probe transitions. Because $NeBr_2$ $\nu'=15$ decays via direct VP, no intermediate species are formed in the predissociation, so the transient peaks should be due to the probe transitions of the initially excited $NeBr_2$. These unassigned probe peaks are not consistent with $NeBr_2$ transitions to excited van der Waals vibrational modes within the $Ne-Br_2$ (E,ν) interaction potentials.[55] Because the $Ne-Br_2$ interaction changes slowly with ν, the location of the van der Waals modes relative to the free Br_2 (E,ν) should also change very slowly with ν. However, the position of the unknown peaks relative to the free Br_2 transitions changes rapidly with ν. In Fig. 4(b), the redshifts of the unknown peaks in the region of $NeBr_2$ $1 \leftarrow 15$ are different from the redshifts of the unknown peaks near $NeBr_2$ $2 \leftarrow 15$, with the redshifts measured relative to the free Br_2 $1 \leftarrow 15$ and $2 \leftarrow 15$ transitions. These unexpected probe transitions also become much less intense with increasing ν; above $\nu=4$, they are hardly visible. This strong dependence on ν leads us to suspect that the extra peaks are due to nonadiabatic interactions with vibronic levels from other ion-pair states induced by the presence of the rare gas atom. Nonadiabatic interactions between halogen ion-pair states induced by rare gas atoms have been observed before,[18,55–58] both in $Rg-X_2$ complexes and in $Rg+X_2$ collisions.

The consequence of these extra peaks for the present study is very congested short delay time probe spectra for Ne_2Br_2 $(B,\nu'<18)$. The congestion is particularly severe for these ν' because probe transitions from these levels have the largest Franck–Condon factors with $(E,\nu=0-3)$, the ν for which the unassigned features are most prominent. The congestion is worsened by the fact that there are transient features from both the initial Ne_2Br_2 and intermediate $NeBr_2$, as will be shown below. We are not reporting time-dependent data on Ne_2Br_2 $\nu'<17$ because the crowded spectra make it difficult to ensure that only one probe transition is being excited and due to uncertainty in assigning the probe transitions. Ideally, we could use probe transitions ending at higher ν, but the small Franck–Condon factors for these transitions did not allow us to achieve useful signal-to-noise ratios.

2. Ne_2Br_2 *probe spectra*

The Ne_2Br_2 probe transitions are assigned using both the established band shift rule from the $NeBr_2$ probe transitions and from the time-dependent behavior of the transitions. Figure 5 shows the probe spectra taken after excitation to Ne_2Br_2 $(B,\nu'=18)$. For a 20 ps pump-probe delay, probe transitions due to the initially excited complex are clearly present: Ne_2Br_2 $E \leftarrow B$, $3 \leftarrow 18$ and $4 \leftarrow 18$. These transitions are 40 and 43 cm^{-1} to the red of the uncomplexed transitions, slightly less than double the 23 cm^{-1} redshift of the corresponding $NeBr_2$ transitions. The Ne_2Br_2 probe transitions are significantly weaker at 60 ps delay, consistent with the assignment to Ne_2Br_2 $\nu'=18$. In the 60 ps delay spectrum a $NeBr_2$ $3 \leftarrow 17$ probe transition is observed. Unlike the Ne_2Br_2 $\nu'=18$ transitions, the $NeBr_2$ $\nu'=17$ peak becomes larger between 20 and 60 ps before finally decaying away at longer delay times. This time-dependent behavior clearly shows that $NeBr_2$ $\nu'=17$ is an intermediate in the predissociation of Ne_2Br_2 $\nu'=18$. From the long time probe spectrum, it is evident that Br_2 $\nu'=16$ is the major product of the Ne_2Br_2 $\nu'=18$ predissociation, with a much smaller decay to $\nu'=15$. Most of the other peaks in the long delay time probe spectrum can be attributed to products of the linear isomer. The $^{81}Br_2$ probe transition is observed from the excitation of a hot band $^{81}Br_2$ $B \leftarrow X$, $22 \leftarrow 1$ transition which overlaps with the $Ne_2{}^{79}Br_2$ $(B,\nu'=18)$ resonance.

These results show the value of the time-resolved spectra in providing details about the dissociation mechanism. The spectra in Fig. 5 indicate that $NeBr_2$ $\nu'=17$ is the dominant intermediate and Br_2 $\nu'=16$ is the dominant product so that Ne_2Br_2 $\nu'=18$ predissociation follows a simple sequential mechanism:

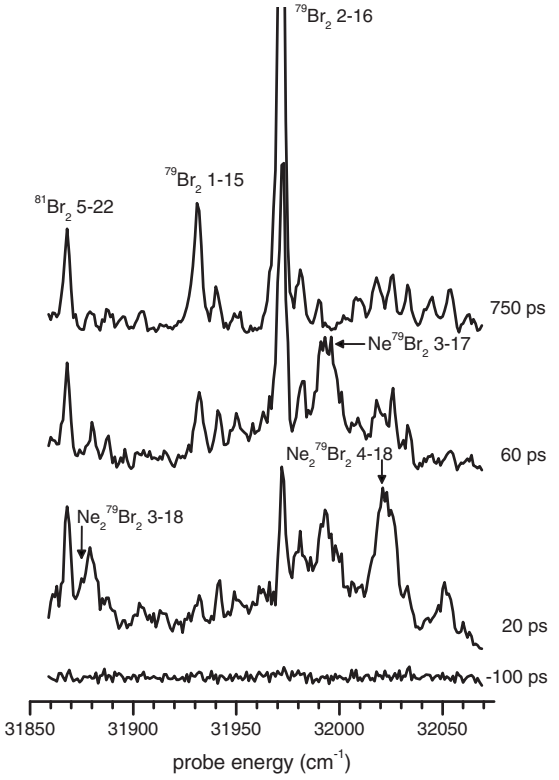

FIG. 5. Probe spectra recorded with the pump pulse fixed to excite Ne_2Br_2 $(B,\nu'=18)$. The labels on the peaks denote the $E\leftarrow B$, $\nu\leftarrow\nu'$ vibronic transitions. Each spectrum is labeled on the right according to the time delay of the probe relative to the pump.

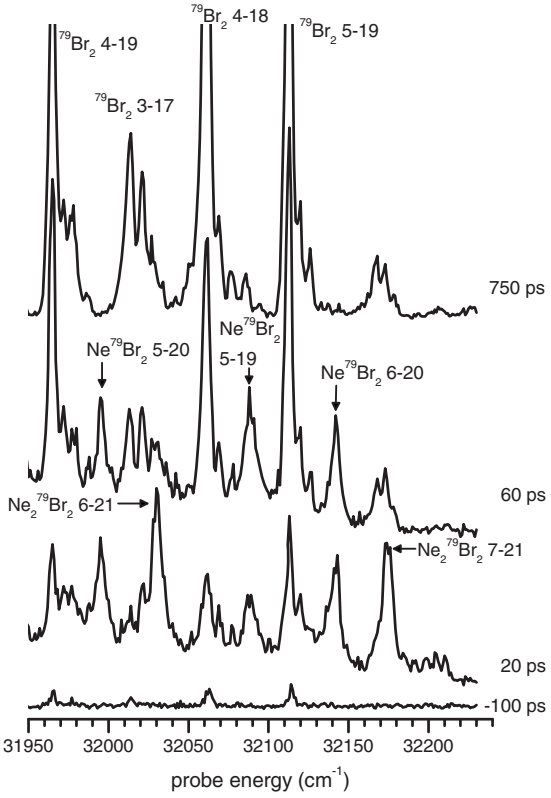

FIG. 6. Probe spectra recorded with the pump pulse fixed to excite Ne_2Br_2 $(B,\nu'=21)$. The labels on the peaks denote the $E\leftarrow B$, $\nu\leftarrow\nu'$ vibronic transitions. Each spectrum is labeled on the right according to the time delay of the probe relative to the pump.

$$Ne_2Br_2(\nu'=18)\rightarrow NeBr_2(\nu'=17)\rightarrow Br_2(\nu'=16).$$

An important check of this conclusion will be in recording the time dependence of all three species and fitting the results to a sequential mechanism.

Figure 6 shows the time-dependent probe spectra after excitation to Ne_2Br_2 $\nu'=21$. These spectra reveal a more complicated dissociation mechanism with multiple pathways. In contrast to Ne_2Br_2 $\nu'=18$ predissociation, $NeBr_2$ $(\nu'-1)$ is not the only intermediate formed; at 60 ps, both $NeBr_2$ $\nu'=20$ and $NeBr_2$ $\nu'=19$ are observed. These multiple pathways are also reflected in the final product state distribution not being predominantly Br_2 $(\nu'-2)$, but instead significant amounts of both Br_2 $\nu'=19$ and $\nu'=18$ are being formed. Extraction of the quantitative ratios for the various product channels is described in the next section.

3. Vibrational product state distributions

From the long delay time probe spectra, we extracted the vibrational product state branching ratios for both $NeBr_2$ and Ne_2Br_2 for initial $16\leq\nu'\leq23$. The results are displayed in Tables I and II. The ratios are taken relative to the first open product channel, which is $(\nu'-1)$ for $NeBr_2$ and $(\nu'-2)$ for Ne_2Br_2 in the range of vibrational levels studied. To obtain these results, the probe power is increased until the probe transitions of all the Br_2 products are saturated. By saturating the probe transitions, the relative intensities of the transitions directly reflect the relative populations of the products, without the need for correcting for the Franck–Condon factors. To remove any contribution to the product peaks from the dissociation of the linear isomer, the intensity of the probe peaks is monitored with the pump laser detuned from the Ne_NBr_2 resonance. The major source of error in these product state distributions is the uncertainty in the intensity of this background, which can be large relative to the intensity of the Ne_NBr_2 resonance when probing the least populated channels. The branching ratios for each ν' were measured at least twice to ensure consistency, and for some levels up to five measurements were done to estimate the random error. The precision of the measurements is quite high, as can be seen from the small standard deviations (shown in parentheses) of the measured values.

For $NeBr_2$, the first open product channel is the domi-

TABLE I. $Br_2(\nu'-n):Br_2(\nu'-1)$ vibrational product branching ratios from the predissociation of $NeBr_2$ (B,ν'). The standard deviations are shown in parentheses for levels where at least four independent measurements were made.

ν'	$(\nu'-1)$	$(\nu'-2)$	$(\nu'-3)$
16	1	0.089	0.011
17	1	0.077 (0.002)	0.009 (0.003)
18	1	0.11 (0.005)	0.012 (0.002)
19	1	0.13 (0.014)	0.013 (0.005)
20	1	0.15 (0.01)	0.024 (0.002)
21	1	0.18	0.032
22	1	0.20 (0.005)	0.043 (0.002)
23	1	0.29 (0.005)	0.069 (0.003)

TABLE II. $Br_2(\nu'-n):Br_2(\nu'-2)$ vibrational product branching ratios from the predissociation of Ne_2Br_2 (B,ν'). The standard deviations are shown in parentheses for levels where at least four independent measurements were made.

ν'	$(\nu'-2)$	$(\nu'-3)$	$(\nu'-4)$	$(\nu'-5)$
16	1	0.16 (0.01)		
17	1	0.31 (0.03)	0.05 (0.01)	
18	1	0.33 (0.04)	0.08 (0.01)	
19	1	0.45 (0.04)	0.09 (0.01)	
20	1	0.65	0.13	0.03
21	1	0.97	0.29	[a]
22	1	1.58 (0.08)	0.51 (0.04)	0.17 (0.02)
23	1	3.28 (0.15)	1.37 (0.06)	0.49 (0.02)

[a]Could not be measured due to spectral congestion.

nant channel for all vibrational levels studied. This is consistent with the predissociation mechanism being predominantly direct VP. However, as ν' gets closer to the closing of the $(\nu'-1)$ channel at $\nu'=27$,[59,60] products from the lower ν' become more important. Experimental vibrational product state distributions of $NeBr_2$ $\nu'=10$, 22, and 27 have been reported before.[59] These measurements were performed via analysis of the dispersed fluorescence spectrum of the product Br_2. So, the results have low precision due to the corrections needed both for collisional relaxation and the rovibrational state dependence of EP in the B state. The pump-probe technique used here avoids these issues. Despite these difficulties, the $(\nu'-2):(\nu'-1)$ product branching ratio for $\nu'=22$ in Ref. 59 is 0.2, the same as we report in Table I. The product branching ratios reported here are also in good agreement with those calculated from a full-dimensional quantum simulation of $NeBr_2$ predissociation.[61]

The Ne_2Br_2 vibrational product state distributions change rapidly with ν'. At lower levels, the first open product channel $(\nu'-2)$ is the dominant channel, but by $\nu'=21$, an almost equal amount of $(\nu'-3)$ is formed. The product state distributions also become broader as ν' increases, with products being observed from $(\nu'-2)$ to $(\nu'-5)$.

C. Delay scans

Figures 7 and 8 show the time-dependent behavior of all the species formed in the VP of Ne_2Br_2 $\nu'=18$ and 21, respectively. These delay scans are obtained by tuning the pump laser to excite Ne_2Br_2 ν', tuning the probe laser to the transitions identified in Figs. 5 and 6, and then scanning the time delay between the pump and probe pulses. To correct for the background signals observed in the excitation scans, a delay scan is collected with the pump laser detuned from the Ne_2Br_2 resonance and then subtracted from the on-resonance delay scan.

The details of the fitting procedure and error analysis can be found in the Appendix and so will only be summarized here. After subtracting the background contribution, the delay scans are fitted assuming a sequential first order kinetic mechanism:

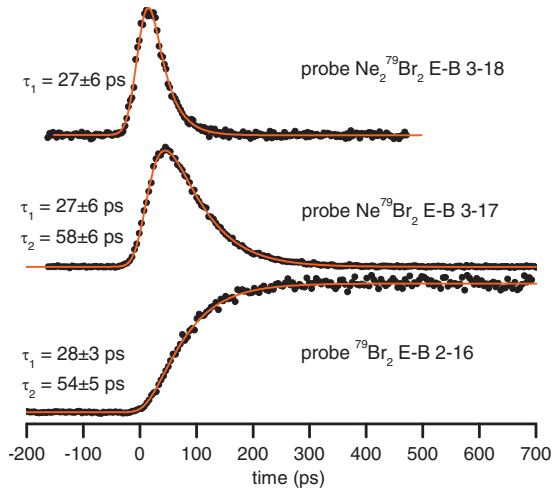

FIG. 7. Delay scans recorded with the pump pulse fixed to excite Ne_2Br_2 $(B,\nu'=18)$ and the probe pulse fixed to detect the initial Ne_2Br_2 $(B,\nu'=18)$, intermediate $NeBr_2$ $(B,\nu'=17)$, and product Br_2 $(B,\nu'=16)$. The red curve shows the fit to the data assuming a sequential first order kinetic mechanism. The time constants listed are those extracted from the fitting procedure.

$$Ne_2Br_2(\nu')\xrightarrow{\tau_1}NeBr_2(\nu'-m)\xrightarrow{\tau_2}Br_2(\nu'-n).$$

The fitting functions are the integrated rate laws of the sequential mechanism convoluted with the Gaussian laser cross-correlation. The values of the time constants τ_1 and τ_2

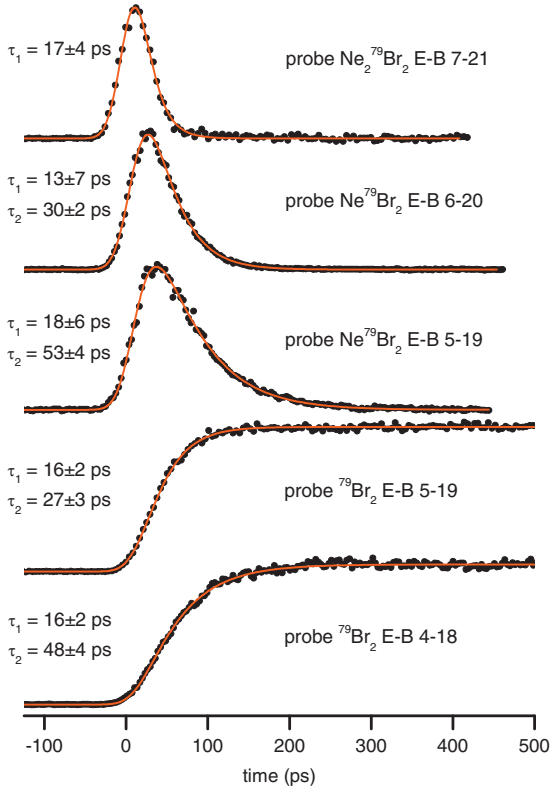

FIG. 8. Delay scans recorded with the pump pulse fixed to excite Ne_2Br_2 $(B,\nu'=21)$ and the probe pulse fixed to detect the initial Ne_2Br_2 $(B,\nu'=21)$, intermediates $NeBr_2$ $(B,\nu'=19,20)$, and products Br_2 $(B,\nu'=18,19)$. The red curve shows the fit to the data assuming a sequential first order kinetic mechanism. The time constants listed are those extracted from the fitting procedure.

TABLE III. Time constants obtained from fits to the delay scans of the species formed in the predissociation of Ne_2Br_2 (B,ν'). The delay scans are fit to a sequential kinetic mechanism $Ne_2Br_2(\nu')\overset{\tau_1}{\rightarrow}NeBr_2(\nu'-m)\overset{\tau_2}{\rightarrow}Br_2(\nu'-n)$. For Br_2 $(\nu'-n)$, the τ_1 values are not obtained from the fit but are fixed to the average value extracted from fits to the Ne_2Br_2 (ν') and $NeBr_2$ $(\nu'-m)$ delay scans. Error bars are 95% confidence intervals. See text for further details.

	Species	τ_1 (ps)	τ_2 (ps)
$\nu'=17$	Ne_2Br_2 $\nu'=17$	32 ± 3	
	$NeBr_2$ $\nu'=16$	30 ± 3	88 ± 3
	Br_2 $\nu'=15$	31 ± 2	82 ± 3
$\nu'=18$	Ne_2Br_2 $\nu'=18$	28 ± 3	
	$NeBr_2$ $\nu'=17$	27 ± 5	58 ± 5
	Br_2 $\nu'=16$	28 ± 3	55 ± 4
$\nu'=21$	Ne_2Br_2 $\nu'=21$	16 ± 3	
	$NeBr_2$ $\nu'=20$	14 ± 5	30 ± 2
	$NeBr_2$ $\nu'=19$	17 ± 4	54 ± 3
	Br_2 $\nu'=19$	16 ± 2	29 ± 2
	Br_2 $\nu'=18$	16 ± 2	47 ± 2

(or, equivalently, rate constants $k_i=1/\tau_i$) that give the best-fit line are found by performing a numerical least-squares minimization.

The time constants obtained from the time-dependent signals due to the species formed in the predissociation of Ne_2Br_2 $\nu'=17$, 18, and 21 are shown in Table III. For each species listed in the table, at least two delay scans were obtained and fitted. The time constant values in Table III are the average of all measurements, with the averaging weighted by the inverse squared error of each measurement. As discussed in more detail in the Appendix, values for τ_1 and τ_2 could not independently be extracted from fits to the Br_2 delay scans due to the background correction. The value listed for τ_1 in the Br_2 scans is the average of the values from the $NeBr_2$ and Ne_2Br_2 delay scans. The value for τ_2 is obtained by fixing τ_1 at this average value when performing the fit.

The sequential mechanism gives an excellent representation of the delay scans, as can be seen from the good agreement between the delay scans and the fit functions in Figs. 7 and 8. The use of the sequential mechanism is further validated by the self-consistency of the fits. For example, the τ_1 values obtained from initial Ne_2Br_2 $\nu'=18$ excitation and $NeBr_2$ $\nu'=17$ intermediate delay scans are 28 and 27 ps, respectively, confirming that the first dissociation step is

$$Ne_2Br_2(\nu'=18)\overset{\tau_1}{\rightarrow}NeBr_2(\nu'=17).$$

Similarly, the τ_2 values for this level are 58 and 55 ps, confirming that the second dissociation step is

$$NeBr_2(\nu'=17)\overset{\tau_2}{\rightarrow}Br_2(\nu'=16).$$

Thus, the dissociation of Ne_2Br_2 $\nu'=18$ can be described by the kinetic mechanism

$$Ne_2Br_2(\nu')\overset{\tau_1}{\rightarrow}NeBr_2(\nu'-1)\overset{\tau_2}{\rightarrow}Br_2(\nu'-2). \quad (1)$$

The time constants for Ne_2Br_2 $\nu'=17$ are also self-consistent, showing that Ne_2Br_2 dissociation can be described by the mechanism in Eq. (1), although the values of τ_2 obtained for $NeBr_2$ $(\nu'=16)$ and Br_2 $(\nu'=15)$ are just outside the error bars of these two values. This may be due to systematic errors from the background correction not accounted for in the error analysis, which only considers random errors.

Examination of the time constant values for the dissociation of Ne_2Br_2 $\nu'=21$ is particularly interesting. Unlike for lower ν', for this level two intermediates are observed: $NeBr_2$ $\nu'=20$ and $\nu'=19$. To within error, the τ_1 values for the initial Ne_2Br_2 and the two intermediates are equal, consistent with $NeBr_2$ $\nu'=20$ and $\nu'=19$ being formed directly from the decay of Ne_2Br_2 $\nu'=21$. $NeBr_2$ $\nu'=20$ and $\nu'=19$ decay at very different rates with τ_2 values of 30 and 54 ps, respectively. Comparison of these τ_2 values to those of the product Br_2 $\nu'=19$ and $\nu'=18$ leads to the conclusion that the final dissociation steps for the formation of the two products are

$$NeBr_2(\nu'=20)\overset{\tau_2}{\rightarrow}Br_2(\nu'=19)$$

and

$$NeBr_2(\nu'=19)\overset{\tau_2}{\rightarrow}Br_2(\nu'=18).$$

Thus, the dissociation of this level follows two different pathways,

$$\begin{array}{l} Ne_2Br_2(\nu')\overset{\tau_1'}{\rightarrow}NeBr_2(\nu'-1)\overset{\tau_2'}{\rightarrow}Br_2(\nu'-2) \\ \quad\downarrow\tau_1'' \\ NeBr_2(\nu'-2)\overset{\tau_2''}{\rightarrow}Br_2(\nu'-3). \end{array} \quad (2)$$

The results presented here represent the most detailed experimental data on the dissociation of a rare gas–halogen complex with more than one rare gas atom attached. Using both the time- and frequency-resolution of our pump-probe experiment, we have been able to characterize not just the first and last steps of the predissociation of the complex, but the intermediate steps as well. In the following, we discuss the implications of the results for determining the predissociation mechanism.

IV. DISCUSSION

A. Model for predissociation dynamics

The goal of this study is to fully characterize the VP dynamics of the Ne_2Br_2 complex. We seek to follow the Br_2 vibrational energy as it flows into the van der Waals "solvent" degrees of freedom, determining what are the steps in the predissociation process, how long these steps take, and how the mechanism of dissociation determines the distribution of final product states. Halberstadt, Bastida, and coworkers developed a kinetic model for describing the flow of vibrational energy in their mixed quantum-classical simulations of Ne_2X_2 predissociation.[34,37,42] In this model, the Br_2 vibrational energy can follow two possible pathways. The vibrational energy can transfer via the direct VP mechanism, with the energy going into a dissociative van der Waals

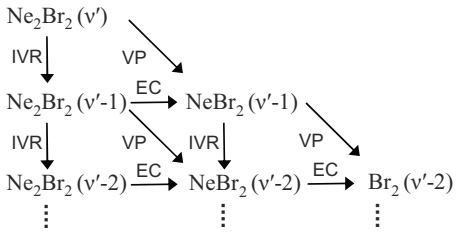

FIG. 9. Kinetic scheme used to describe the possible predissociation mechanisms of Ne_2Br_2. In this model the loss of each vibrational quantum can proceed via direct VP or IVR. Each Ne atom is lost either through direct VP or through EC following IVR. Adapted from Fig. 1 of Ref. 37.

stretching mode and immediately dissociating a Ne atom. The second possibility is IVR, with the vibrational energy flowing into a nondissociative van der Waals mode so that no dissociation takes place. Following the IVR step, the excess van der Waals energy may transfer from the excited nonreactive mode to a reactive mode, "boiling off" a Ne atom in a process called evaporative cooling (EC), or a second vibrational quantum may be transferred to this excited Ne_2Br_2 $(\nu'-1)$ complex, leading to further IVR and VP. These possible dissociation pathways are summarized in Fig. 9. This kinetic model provides a useful framework for describing the dissociation mechanism and will be used in the following discussion.

There are a few caveats to this model. First, it gives a classical picture of the dissociation, ignoring quantum interference among the various pathways. Second, it does not consider more than one quantum of vibrational energy being simultaneously transferred in one step because this is a much less likely process. Studies on the dissociation of RgX_2 (ν') complexes that require more than one quantum to dissociate show that the quanta are transferred sequentially rather than simultaneously,[9,47] so that these complexes dissociate via an IVR intermediate formed after the transfer of the first quantum rather than a direct VP mechanism. Full-dimensional quantum calculations on Ne_2I_2 $\nu'=21$ predissociation show the same thing, with the simultaneous loss of two quanta being an order of magnitude less likely than the loss of one quantum.[45]

B. Energy changes with ν'

The results show that the dissociation dynamics change rapidly over the range of initial $16 \leq \nu' \leq 23$ studied. For $\nu' \leq 19$, the major intermediates and products formed are $NeBr_2$ $(\nu'-1)$ and Br_2 $(\nu'-2)$. For higher ν' levels, multiple $NeBr_2$ $(\nu'-m)$ are observed, and product Br_2 from levels lower than $(\nu'-2)$ becomes much more important. Because the $Ne-Br_2$ and Ne–Ne interactions change negligibly with ν', the important cause of these changes in dissociation mechanism with ν' is the decrease of the Br_2 stretching quanta with increasing ν'. The energy of individual Br_2 stretching quanta decreases from 108 cm^{-1} for $\nu'=16$ to 79 cm^{-1} for $\nu'=23$. Before discussing the probable dissociation mechanisms of Ne_2Br_2 (B,ν'), the energetics will be examined to note the possible reaction channels. For example, the direct VP $\Delta\nu'=-1$ pathway cannot be considered if one quantum of vibrational energy is insufficient to remove the rare gas atom for an initially excited ν' level.

In order for the first vibrational quantum transferred to remove a Ne atom from the Ne_2Br_2 complex, both a $Ne-Br_2$ and the Ne–Ne bond must be broken. We estimate the energy required for the dissociation step to be the sum of the $Ne-Br_2$ and Ne–Ne binding energies. The $Ne-Br_2$ binding energy for $16 \leq \nu' \leq 23$ is $D_0=62$ cm^{-1}.[60] Adding the Ne–Ne D_0 of 17 cm^{-1},[37,62] it takes 79 cm^{-1} to remove the first Ne atom. Adding to this quantity the 62 cm^{-1} needed to dissociate the second atom, the total binding energy of the Ne_2Br_2 complex is then 141 cm^{-1}. This estimate should be accurate. Villarreal *et al.*[24] calculated the Ne_2I_2 binding energy and found that the exact value is within 1 cm^{-1} of the value obtained by summing the D_0 values.

Using these values, the Br_2 vibrational levels can be identified for which various dissociation steps become energetically forbidden. As noted in the results, $\nu'=27$ is the last level for which one quantum can dissociate the $NeBr_2$ complex because the vibrational energy gap at Br_2 $(B,\nu'=27)$ is 63 cm^{-1}, barely enough energy to dissociate the complex into $Ne+Br_2$ $(B,\nu'=26)$. Similarly, in the Ne_2Br_2 complex, the loss of the first Ne atom via the transfer of one vibrational quantum would close above $\nu'=23$ since the energy gap at this level is 79 cm^{-1}. The dissociation of Ne_2Br_2 into $2\ Ne+Br_2$ $(\nu'-2)$ would close above $\nu'=25$ assuming a binding energy of 141 cm^{-1}. Combining these considerations of the energetics with the experimental results, we can determine the likely dissociation pathways. To the extent that IVR broadens the excitation bands, the energetic thresholds become less defined.

C. Dissociation mechanism for low ν' levels

For the low ν' levels of Ne_2Br_2, the major intermediate is $NeBr_2$ $(\nu'-1)$ and the major product is Br_2 $(\nu'-2)$. The dissociation pathway that is consistent with this observation is the one which consists of two direct VP steps,

$$Ne_2Br_2(\nu') \xrightarrow{VP} NeBr_2(\nu'-1) \xrightarrow{VP} Br_2(\nu'-2). \quad (3)$$

Further evidence of the sequential direct VP pathway is that the time-dependent behavior is well-described by a single sequential kinetic scheme [Eq. (1)]. All other possible pathways include an IVR step that would in most cases lead to multiple intermediates and products in lower vibrational levels. It is unlikely, for example, that a pathway described by two sequential IVR steps to form Ne_2Br_2 $(\nu'-2)$, followed by EC to remove both Ne atoms, is a significant contributor to the final $(\nu'-2)$ product. It is also unlikely that such an IVR pathway would yield the distinct intermediate resonance probe spectra observed here.

A second pathway consistent with our observations is that a Ne_2Br_2 $(\nu'-1)$ intermediate decays into $NeBr_2$ $(\nu'-1)$ (the IVR-EC mechanism). In order for the experimental observations to agree with this mechanism, the Ne_2Br_2 $(\nu'-1)$ intermediate would have to be very short-lived since the sequential VP mechanism fits the observed dynamics extremely well. However, this IVR-EC possibility is most

likely not important for lower ν' because the results show that the other IVR pathways (IVR followed by either VP or further IVR) are not significant.

It is reasonable that VP predominates over IVR for these levels, considering that the number of nondissociative "solvent" degrees of freedom is low and can only accept a limited amount of energy. The vibrational energy gaps at low ν' are sufficiently large so that there is more than enough energy to remove the first Ne atom even if some of the vibrational energy goes into nondissociative van der Waals modes. For Ne_2Br_2 $\nu'=18$, one quantum of Br_2 vibration is 100 cm^{-1}. If an IVR mechanism was to occur for this level, more than 21 cm^{-1} of energy would need to flow into the nonreactive van der Waals vibrational modes to avoid dissociating a Ne atom when the first quantum is transferred. However, this does not preclude the possibility that some vibrational energy is transferred to nondissociative modes so that the $NeBr_2$ $(\nu'-1)$ intermediate is formed with excess energy in its van der Waals degrees of freedom.

D. Dissociation mechanism for high ν' levels

The increasing proportion of the product formed at levels below $(\nu'-2)$ as ν' increases could indicate that dissociation via IVR is more probable at higher ν'. Using the kinetic model in Fig. 9, IVR leads to lower $(\nu'-n)$ products because the vibrational quanta go into nonreactive degrees of freedom. For example, the presence of Br_2 $(\nu'-3)$ indicates that the dissociation may be occurring via the pathway

$$\mathrm{Ne_2Br_2}(\nu') \xrightarrow{\mathrm{IVR}} \mathrm{Ne_2Br_2}(\nu'-1) \xrightarrow{\mathrm{VP}} \mathrm{NeBr_2}(\nu'-2) \xrightarrow{\mathrm{VP}} \mathrm{Br_2}(\nu'-3). \quad (4)$$

From Fig. 9, it is clear that there are many other pathways that lead to the Br_2 $(\nu'-3)$ product other than that shown in Eq. (4), but most are not consistent with the observed intermediates and time-dependent behavior of the dissociation mechanism.

For $\nu'=21$, the vibrational product state distributions show that IVR and VP pathways are in competition, with almost equal amounts of Br_2 $(\nu'-2)$ and $(\nu'-3)$ being formed. The observed time-dependent behavior of the dissociation illustrates this branched behavior [Eq. (2)]. The VP pathway is the branch leading to the formation of the $NeBr_2$ $(\nu'-1)$ intermediate and Br_2 $(\nu'-2)$ product, as was observed for the lower ν'. The IVR pathway is the branch yielding $NeBr_2$ $(\nu'-2)$ intermediate and Br_2 $(\nu'-3)$ product. Because losing the first quantum via IVR is a likely process for $\nu'=21$, it also may be probable that the $NeBr_2$ $(\nu'-1)$ is formed via IVR-EC as well as direct VP, although the Ne_2Br_2 $(\nu'-1)$ IVR intermediate would have to be very short-lived to be consistent with the observed kinetics. The Ne_2Br_2 $(\nu'-1)$ intermediate is discussed in further detail below.

The IVR pathway of $\nu'=21$ is significantly more important than for lower levels because the amount of vibrational energy available is much smaller. One Br_2 stretching quantum at $\nu'=21$ contains 88 cm^{-1} of energy, only 9 cm^{-1} above the threshold for the loss of the first Ne atom. Thus, the results indicate it is probable for at least 9 cm^{-1} of vibrational energy to go into the nonreactive modes so that there is no longer enough energy in the reactive modes for direct VP to occur.

The IVR branch of the kinetic model [Eq. (4)] assumes the existence of the intermediate Ne_2Br_2 $(\nu'-1)$, which then decays into $NeBr_2$ $(\nu'-2)$ via VP and $NeBr_2$ $(\nu'-1)$ via EC. However, we did not observe this IVR intermediate. Instead, the time-dependent behavior is consistent with the initial Ne_2Br_2 (ν') decaying directly into $NeBr_2$ $(\nu'-1)$ and $(\nu'-2)$. One possibility is that the Ne_2Br_2 $(\nu'-1)$ intermediate decays very rapidly into the observed $NeBr_2$ $(\nu'-2)$ intermediate. Because of the 35 ps time resolution of the experiment, Ne_2Br_2 $(\nu'-1)$ could have a lifetime as long as ≈ 5 ps without being detected in the time-dependent data. The existence of a short-lived intermediate is reasonable. Similar intermediates have been calculated for the dissociation of $NeBr_2$ just below the closing of the $(\nu'-1)$ product channel.[61,63–65] In that case, the intermediate $NeBr_2$ $(\nu'-1)$ is in a highly excited bending state supported by a centrifugal barrier. The IVR intermediate decays into Br_2 $(\nu'-2)$ and is responsible for the increasing importance of the $\Delta\nu'=-2$ channel as ν' approaches the closing of the $\Delta\nu'=-1$ channel at $\nu'=27$ (Table I).

Another reason that the Ne_2Br_2 $(\nu'-1)$ intermediate may not be observed is that its probe spectrum is probably broad and weak. Very little is known about the $E \leftarrow B$ transitions of the rare gas-halogen complexes with excitation in the van der Waals modes.[18,55] However, it is reasonable that an excited van der Waals mode of Ne_2Br_2 $(\nu'-1)$ would be highly delocalized and therefore have small Franck–Condon overlap with many van der Waals states within each (E,ν) interaction potential. Also, the density of van der Waals states of Ne_2Br_2 $(\nu'-1)$ would likely be high so that its probe spectrum would contain many very weak $E \leftarrow B$ transitions between excited van der Waals modes in the $(B,\nu'-1)$ and (E,ν) potentials.

Despite the lack of a directly observed IVR intermediate, the results presented here strongly support the IVR mechanism becoming significantly more important. The other possibility, the simultaneous transfer of multiple quanta of Br_2 vibrational energy, is a much less likely process. An examination of the $NeBr_2$ product state distribution at higher ν' might lead to the conclusion that the simultaneous transfer of two quanta becomes more likely since the $(\nu'-2)$ channel increases in importance even though the $(\nu'-1)$ channel is still open. However, as discussed in the previous paragraph, this $(\nu'-2)$ channel is formed via a $NeBr_2$ $(\nu'-1)$ intermediate, albeit a very short-lived one. The products of Ne_2Br_2 dissociation (Table II) also can populate very low vibrational levels, all the way down to $(\nu'-5)$. Creating these products via the simultaneous loss of more than two quanta would be improbable, and an IVR mechanism is much more reasonable. The loss of five quanta of vibrational energy may indicate that the IVR intermediate is in a highly excited bending mode in which a Ne atom samples the linear configuration, where the transfer of multiple vibrational quanta is very efficient.[48]

TABLE IV. Comparison of the lifetimes of the Ne_2Br_2 (B,ν') complex (the τ_1 values in Table III) to the lifetimes of the $NeBr_2$ (B,ν') complex.

ν'	$\tau_{Ne_2Br_2}$ (ps)	τ_{NeBr_2} (ps)[a]
17	32±3	49±3
18	28±3	42±2
21	16±3	23±2

[a]From Ref. 11 for $\nu'=17$ and 18.

E. Comparison to $NeBr_2$ predissociation lifetimes

In Table IV we compare the Ne_2Br_2 (ν') lifetimes (the τ_1 values shown in Table III) to the $NeBr_2$ (ν') lifetimes obtained by fitting the Br_2 $(\nu'-1)$ product appearance delay scan to a single exponential rise function. The $NeBr_2$ values were first reported in Ref. 11, except for $\nu'=21$, which is being reported here for the first time. If the two Ne atoms were independent of each other, Ne_2Br_2 (ν') direct VP lifetimes would be half those of the corresponding $NeBr_2$ (ν') lifetimes (τ_{NeBr_2}). Likewise, the couplings between the Br_2 stretch and van der Waals stretch would be the same as in the $NeBr_2$ complex, but the two Ne atoms double the probability of dissociation in a given time interval.[23]

In the case of the He_2X_2 complexes, the negligible He–He interaction allows the predissociation to be well-described assuming the He atoms are independent within the complex. This independence is reflected both in the strong propensity to lose only one He atom per vibrational quantum transferred and in the observed predissociation rates. For example, the calculated and experimental predissociation rates of the He_2Cl_2 $\nu'=10-13$ are very close to twice the rates of the corresponding $HeCl_2$ $\nu'=10-13$ rates.[13,21,26]

However, the Ne–Ne interaction is not negligible so that this assumption of independence probably breaks down. Two consequences of the Ne–Ne interaction are (1) the product Ne atom kinetic energy for the first dissociation step will be lower and (2) coupling leading to IVR resonances is more likely. Each of these two effects would be expected to increase the rate for the first dissociation step compared to the "independent Ne" model.

Thus, the results in Table IV are somewhat surprising: the Ne_2Br_2 lifetimes are unexpectedly long. While all the Ne_2Br_2 lifetimes are shorter than those of the corresponding $NeBr_2$, the lifetimes are all longer than $\frac{1}{2}\tau_{NeBr_2}$. The measured rate for Ne_2Br_2 $\nu'=21$ is especially surprising. For this level, significant IVR is occurring, so we would expect a lifetime shorter than $\frac{1}{2}\tau_{NeBr_2}$ due to the multiple dissociation pathways. However, the observed 16 ps decay time is longer than $\frac{1}{2}\tau_{NeBr_2}=11$ ps. Gutmann *et al.*[23] observed a similar slowdown in the Ne_2I_2 dissociation.

As discussed in Ref. 23, the direct VP lifetime is $\frac{1}{2}\tau_{NeX_2}$ only if the Ne_2X_2 van der Waals modes can be described as two independent Ne-X_2 local modes. That is, a direct product of Ne-X_2 van der Waals wave functions provides a good zero-order description of the Ne_2X_2 van der Waals wave function. If so, the coupling between the X_2 stretch and the Ne-X_2 local mode is identical for both the triatomic and tetratomic complexes, but the rate is twice as fast in the latter since there are two local modes. That the overall Ne_2X_2 (direct VP plus IVR) predissociation lifetime is greater than $\frac{1}{2}\tau_{NeBr_2}$ indicates that the direct VP rate is significantly smaller than predicted by the "independent Ne" model. This local mode picture breaks down due to the strong Ne–Ne interactions, so predicting the Ne_2X_2 direct VP rates from NeX_2 direct VP rates is not possible.

TABLE V. Comparison of the lifetimes of the $NeBr_2$ $(B,\nu'-m)$ intermediates (τ_{inter}) formed in the predissociation of Ne_2Br_2 (B,ν') to the lifetimes of the $NeBr_2$ $(B,\nu'-m)$ prepared via direct laser excitation (τ_{direct}).

ν'	$\nu'-m$	τ_{inter} (ps)	τ_{direct} (ps)[a]
17	16	88±3	68±3
18	17	58±5	49±2
21	20	30±2	29±4
	19	54±3	35±3

[a]From Ref. 11.

Another possible cause for this unexpected result is that the product wave functions and dissociation channels for the loss of a Ne atom from Ne_2Br_2 will be quite different from those of the $NeBr_2$ dissociation for the same level. It takes more energy to eject the Ne atom from Ne_2Br_2, and some of the product channels involve van der Waals excitations of the remaining $NeBr_2$. In a perturbation theory description, the matrix elements between the initial and final states may then be smaller than expected from the independent Ne model.

In Table V we compare the decay times of the $NeBr_2$ $(\nu'-m)$ intermediates formed from the dissociation of Ne_2Br_2 (ν') (the τ_2 values shown in Table III) to $NeBr_2$ $(\nu'-m)$ lifetimes obtained by directly exciting the $NeBr_2$ to the $(\nu'-m)$ vibrational level. The $NeBr_2$ $(\nu'-m)$ prepared by direct laser excitation is in its ground van der Waals state. However, as discussed above, the $NeBr_2$ $(\nu'-m)$ intermediates are likely formed with excitation in the van der Waals modes and so may have different lifetimes.

As can be seen in the table, for some of the ν' levels there is a large difference in lifetime. The $NeBr_2$ $(\nu'-1)=16$ complex formed from the dissociation of Ne_2Br_2 $\nu'=17$ has a lifetime of 88 ps, much longer than the 68 ps lifetime of the same complex prepared via direct laser excitation. Similarly, the $NeBr_2$ $(\nu'-2)=19$ formed in the dissociation the Ne_2Br_2 $\nu'=21$ has a lifetime of 54 ps, while the directly excited complex has a 35 ps lifetime. In contrast, the other intermediate formed in the predissociation of Ne_2Br_2 $(\nu'=21)$, the $NeBr_2$ $(\nu'-1)=20$ complex, has a lifetime identical to the directly excited complex. This observation supports the notion that the difference in lifetimes is due to the intermediates being formed with excess van der Waals energy. As noted above, there is only 9 cm^{-1} of excess energy available to form $NeBr_2$ $(\nu'-1)=20$ from Ne_2Br_2 $\nu'=21$, so that this intermediate is formed with little or no van der Waals vibrational excitation, and thus is similar if not identical to the "cold" $NeBr_2$ $(\nu'-1)=20$ complex prepared by the laser. There is an extra quantum of energy available in the formation $NeBr_2$ $(\nu'-2)=19$, so this intermediate is formed with greater van der Waals excitation. The van der Waals excitation leads to a longer lifetime, as predicted by

Halberstadt and co-workers for $NeCl_2$.[66] The reason for this increased lifetime is that the Ne atom with stretching or low-amplitude bending excitation spends less time near the Br_2, where the coupling responsible for VP is the greatest. For highly excited bending motions that sample the linear configuration, the lifetime may decrease due to the stronger coupling in the linear region. Thus, it would be interesting to record the time-dependent behavior of the $\nu'-5$ product which, as noted above, may be formed via such a large-amplitude bending mode. Unfortunately, recording the desired data will be difficult due to poor signal-to-noise ratios for this product.

Despite the lifetimes strongly indicating that the $NeBr_2$ intermediates are formed with excess energy in the van der Waals modes, the width and redshift of the corresponding probe transitions are not significantly different from those of the $NeBr_2$ prepared by direct excitation with no excess energy in the van der Waals modes. The probable reason for this small change is that the $NeBr_2$ intermediates are in the lowest van der Waals levels just above the van der Waals ground state, and the transition energies of excitations from low-lying van der Waals levels in the (B,ν') intermolecular potential to low-lying levels in the (E,ν) potential are similar to the $E \leftarrow B$ transitions between the ground van der Waals levels. There very likely is a difference between the probe transitions of the unexcited and excited $NeBr_2$ intermediates, but the difference is too small for us to see with the 2 cm^{-1} resolution of the probe pulse.

Considering that the vibrational energy gap decreases by only 4 cm^{-1} from $\nu'=17$ to $\nu'=18$, it would be expected that a similarly large difference in lifetime would be observed between the $NeBr_2$ $\nu'=17$ intermediate and the directly excited complex, as was observed for the $NeBr_2$ $\nu'=16$ intermediate and its partner. However, for $NeBr_2$ $\nu'=17$ the error bars on the lifetimes nearly overlap (58 ± 5 ps for the intermediate versus 49 ± 3 ps for the directly excited complex). The difference is even smaller if the comparison is made to the intermediate decay time (τ_2) extracted from the Br_2 $\nu'=16$ product formation (55 ± 4 ps).

Gutmann *et al.*[23] did not observe significant differences between the decay of the NeI_2 intermediate and the directly excited NeI_2. This discrepancy may be due to energetics. They studied Ne_2I_2 over the range of $17\leq\nu'\leq23$. The vibrational energy gap of I_2 at $\nu'=17$ is 97 cm^{-1}.[67] Since the dynamics is mainly determined by the amount of excess energy, Ne_2Br_2 $\nu'=18$ should be similar to the I_2 complex since the energy gap at $\nu'=18$ is 100 cm^{-1}. Assuming the $Ne-I_2$ binding energy is close to the $Ne-Br_2$ binding energy,[68] the amount of excess energy for both complexes in these vibrational levels should be comparable. As was discussed in the previous paragraph, the difference in lifetime between the $NeBr_2$ $\nu'=17$ intermediate and directly excited complex is small, consistent with what was found by Gutmann *et al.* for the intermediate NeI_2 $\nu'=16$ formed during Ne_2I_2 $\nu'=17$ predissociation. At higher I_2 ν', the energy gaps are even smaller, leading to a greater propensity to form "cold" NeI_2 that is similar to the NeI_2 prepared via direct laser excitation.

F. Comparison to theory

A major motivation for the present work is providing detailed experimental data on the dissociation of larger rare gas–halogen complexes that can serve as benchmarks for approximate computational methods. The only theoretical study performed for Ne_NBr_2 was done by Miguel *et al.* using the molecular dynamics with quantum transition (MDQT) methodology.[37] In these calculations the time-dependent behavior of the Br–Br degree of freedom was treated quantum mechanically, and the van der Waals degrees of freedom were treated classically. The results were fit to the model shown in Fig. 9 to determine the fraction of trajectories following each pathway. Qualitatively, the calculated results are in good agreement with the experimental results. The MDQT simulations predict the Ne_2Br_2 $\nu'=17$ decay time to be about 30 ps, very close to the experimental value of 32 ps. The calculations also show the same trend in the dissociation mechanisms with ν' as we have observed experimentally. For low ν', direct VP is the primary means by which the first quantum is lost, but IVR becomes more important with increasing ν'. However, the calculations show IVR becoming important at much lower ν' values than indicated by the experiment. At $\nu'=17$, the MDQT simulations predict that only 16% of the trajectories proceed via direct VP; the rest proceed via IVR. The MDQT results indicate that IVR-EC accounts for nearly 38% of all trajectories for $\nu'=17$. The experiment cannot distinguish IVR-EC from direct VP if the IVR intermediate is short-lived. However, the experimental result that 86% of Ne_2Br_2 $\nu'=17$ decays via $\Delta\nu'=-2$ is strong evidence that IVR is not important for this level (Table II). The MDQT results show that even for Ne_2Br_2 $\nu'=14$, the $\Delta\nu'=-2$ decay is already only 80%. It will be interesting to explore whether the reason the MDQT results differ from the experiment is due to inadequate potential energy surfaces or due to a more fundamental limitation of the method.

G. Comparison to other Ne_2X_2 complexes

Comparing the data presented here for Ne_2Br_2 predissociation to that of Ne_2Cl_2 and Ne_2I_2, some general conclusions can be drawn regarding the predissociation mechanisms for these Ne_2X_2 complexes. As has been discussed, the mechanism(s) of predissociation are strongly determined by the size of the vibrational energy gap. So, the likely predissociation mechanisms can be grouped into different energy regimes. Denoting the amount of energy in losing n vibrational quanta from X_2 ν' as $E(\nu'-n)$, the following classification of energy regimes seems appropriate:

(1) $E(\nu'-1)>D_0(Ne_2X_2)$. In this regime, one quantum is enough energy to remove both Ne atoms. Because the Ne atoms are not independent of each other, the vibrational energy can be transferred to both Ne-X_2 dissociative stretching modes, leading to the formation of X_2 $(\nu'-1)$. This is observed in the predissociation of Ne_2Cl_2 $(\nu'<9)$.[14] Using the model in Fig. 9, the vibrational quantum transferred may initially go into nonreactive modes before the highly excited Ne_2X_2 $(\nu'-1)$

boils off both Ne atoms via evaporative cooling. He_2X_2 complexes are almost always studied in this energy regime due to their small binding energies, but unlike the Ne complexes they usually lose one quantum per Rg atom, reflecting the independence of the He atoms within the complex. For very low ν' levels of Ne_2X_2, it would be interesting to see if, as with He_2X_2, the energy gap is too large for any intermediate Ne_2X_2 $(\nu'-1)$ to exist, so that the individual Ne atoms behave more independently.

(2) $D_0(Ne-NeX_2) \ll E(\nu'-1) < D_0(Ne_2X_2)$. In this regime, one quantum of energy is more than enough to remove one Ne atom but not large enough to remove both Ne atoms. The dissociation mechanism is primarily sequential direct VP, as is observed here for Ne_2Br_2 $\nu'=16-18$. This also is the likely dissociation mechanism of Ne_2Cl_2 $(\nu' \geq 9)$, just above the closing of the $\nu'-1$ product channel. Consistent with sequential direct VP, the primary product formed is Cl_2 $(\nu'-2)$.[14]

(3) $D_0(Ne-NeX_2) \leq E(\nu'-1)$. If the energy in the first quantum is slightly larger than the energy required to remove the first Ne atom, IVR can occur if enough energy is transferred to the nonreactive modes such that there is not sufficient energy in the reactive modes to break the van der Waals bond via direct VP. In this case, direct VP and IVR are in competition, as we observed for Ne_2Br_2 at higher ν'. This is likely the situation as well for Ne_2I_2 $\nu'=21$. For this level, both product I_2 $(\nu'-2)$ and $(\nu'-3)$ are observed, consistent with direct VP and IVR in competition. For I_2 $\nu'=21$, $E(\nu'-1)=89$ cm^{-1},[67] small enough that IVR is expected to be important.

(4) $D_0(Ne-NeX_2) > E(\nu'-1)$. When the first vibrational quantum is no longer sufficient to remove the Ne atom, direct VP can no longer occur, so the loss of the first quantum must proceed via IVR.

Thus, the Ne_2X_2 complexes undergo a variety of vibrational energy transfer processes, from the relatively simple direct VP process to more complicated IVR mechanisms. Besides vibrational dynamics, electronically nonadiabatic dissociation mechanisms likely occur as well. Taylor *et al.*[11] showed that $NeBr_2$ undergoes significant EP for $\nu'=11$, 13, and 14. The addition of a second Ne atom should further enhance the nonadiabatic coupling between Br_2 electronic states. It will be very interesting to study the EP process for complexes involving more than one rare gas atom. By judicious choice of ν', we can select which electronic and vibrational dynamics to explore in the Ne_2Br_2 complex. As with many other rare gas–halogen complexes, the Ne_2Br_2 complex has proven to be an extremely interesting model system for a wide range of dynamics.

V. CONCLUSION

We report the first direct measurements of the time dependence of intermediates in the dissociation process for a Rg_2X_2 species via time-dependent pump-probe spectroscopy. Because we want to distinguish between competing dissociation pathways, we have taken great care to obtain large signal-to-noise ratios for the time-dependent data and to achieve the lowest possible uncertainty in the measured lifetimes. This goal is difficult because of background signals for other isomers and dynamical processes occurring in the ion-pair electronic states we use for our probe signals.

For the $16 \leq \nu' \leq 23$ levels of the distorted tetrahedral isomer of the Ne_2Br_2 B state, the dissociation kinetics is completely consistent with a two-step mechanism in which the Ne atoms are dissociated sequentially. This kinetic model gives excellent fits to the time dependence of the transients and products that are observed. For the lower ν' levels, the dissociation proceeds via two direct VP steps, and $(\nu'-2)$ final product states are dominant. For the higher ν' levels, both $(\nu'-1)$ and $(\nu'-2)$ channels are observed for loss of the first Ne atom, and final product channels down to $(\nu'-5)$ are observed. Thus, it is clear that intramolecular vibrational energy relaxation plays an important role for these levels.

Although the two-step model provides an accurate fit to the data, interference from signals due to the linear $NeBr_2$ isomer and, probably, the "police nightstick" isomer of Ne_2Br_2 complicates the analysis of the experiments. Any decay channel for the tetrahedral Ne_2Br_2 isomer that is much faster than those discussed here could be masked by these background signals. However, the observation of strong intermediate probe transitions and the self-consistency of the time constants obtained from the sequential mechanism fits indicate that mechanisms other than the sequential one play a minor role in the overall dynamics of the levels studied here.

A particularly noteworthy result of these studies is that the dissociation rates of the initially excited Ne_2Br_2 levels are slower than twice those of the same $NeBr_2$ levels, with the doubling of the dissociation rate expected if the two Ne atoms were independent. The onset of IVR and the higher dissociation energy for Ne_2Br_2 relative to $NeBr_2$ might have been expected to accelerate the rate beyond the independent atom model. Instead, the rates are slower. Another interesting result is that the lifetime of the $NeBr_2$ intermediate resulting from dissociation of a Ne atom from Ne_2Br_2 is always equal to or greater than the lifetime of the same ν' level of $NeBr_2$ produced by direct excitation. The two lifetimes tend to be equal when the Ne_2Br_2 first dissociation step leaves little internal energy in the $NeBr_2$ intermediate, and greater when there is excess internal energy. This implies that van der Waals excitation of the $NeBr_2$ degrees of freedom results in slower dissociation rates. This has been predicted previously, based on a longer $Ne-Br_2$ bond length for excited van der Waals vibrational levels.

The results presented here are the most detailed dynamical description of any Rg_2X_2 van der Waals cluster. Along with the results available for the T-shaped and linear isomers of $NeBr_2$, including the competition between direct VP and EP of low vibrational levels of $NeBr_2$,[11] the Ne_NBr_2 system offers a wealth of data for testing both electronic structure and dynamical theory. The approximate dynamics calculations currently available for Ne_2Br_2 appear to overstate the importance of IVR. It remains to be seen if this is due to too much coupling between the Ne and Br_2 in the potential energy surface or if it is a result of the dynamical approximation. Although not analyzed in detail in this paper, the results

presented here also indicate that there are electronically nonadiabatic effects to be studied in the ion-pair excited states of $NeBr_2$.

ACKNOWLEDGMENTS

We thank N. Halberstadt for the helpful discussion and comments. C.R.B. acknowledges support from the Hewlett-Mellon Faculty Development Fund of Albion College. This work has been supported by the U.S. National Science Foundation, Awards Nos. CHE-0404743 and CHE-0911686.

APPENDIX: FITTING PROCEDURE AND ERROR ANALYSIS FOR DELAY SCANS

As noted in Sec. III, extracting the dissociation time constants from fits to the delay scans was complicated by the time-dependent background signals. Here the procedure used for obtaining the time constants and for quantifying the error introduced by the background correction and other experimental uncertainties is given in detail.

To correct for the background signal, a "background-only" delay scan is obtained by detuning the pump laser from the Ne_2Br_2 resonance. The background is assumed to vary slowly with frequency so that the ≈ 10 cm^{-1} detuning gives a good representation of the background underneath the Ne_2Br_2 resonance. The background-corrected delay scans (obtained by subtracting the off-resonance scan from the on-resonance scan) are fitted assuming a sequential first order kinetic mechanism:

$$Ne_2Br_2(\nu') \overset{\tau_1}{\rightarrow} NeBr_2(\nu'-m) \overset{\tau_2}{\rightarrow} Br_2(\nu'-n).$$

The fitting functions $F(t)$ are the integrated rate laws $I(t)$ of the sequential mechanism convoluted with the Gaussian laser cross-correlation:

$$F(t) = b_0 + A_0 \int_{-\infty}^{t-T_0} \exp\left(\frac{-t'^2}{2\sigma_{CCT}^2}\right) I(t-t'-T_0)dt'. \quad \text{(A1)}$$

The parameters b_0 and A_0 are for fitting the background and overall scale of the data. T_0 is the time t where the delay between the pump and probe pulses is zero. The cross-correlation width σ_{CCT} and T_0 are measured by recording delay scans with the pump and probe pulses tuned to excited a Br_2 double resonance: Br_2 $E \leftarrow B \leftarrow X$, $\nu \leftarrow \nu' \leftarrow 0$. The best-fit parameters are found by numerically minimizing the sum-squared error between the background-corrected delay scans and the fit functions. For the delay scans probing the Ne_2Br_2 (ν') decay, the fitting parameters are A_0, T_0, and τ_1. For the $NeBr_2$ $(\nu'-m)$ delay scans, the fitting parameters are A_0, T_0, τ_1, and τ_2. The Ne_2Br_2 (ν') and $NeBr_2$ $(\nu'-m)$ scans are independently fitted.

Since the Br_2 formation is a result of a multistep dissociation process, the signal at a short delay time is dominated by the background signal. Thus, the background correction creates a large uncertainty in the best-fit values. There is also a much stronger correlation among the τ_1, τ_2, and T_0 parameters compared to the Ne_2Br_2 and $NeBr_2$ traces. Because of these features, the Br_2 $(\nu'-n)$ scans are fit with the τ_1 fixed at the average value of the τ_1 values extracted from the corresponding Ne_2Br_2 (ν') and $NeBr_2$ $(\nu'-m)$ scans. The only parameters allowed to vary are τ_2 and T_0.

Another challenge was obtaining consistent values for T_0. The T_0 measured in the Br_2 double resonance delay scans and the T_0 in the delay scans of the Ne_2Br_2 (ν') predissociation should be the same. Typically they differed by less than 5 ps, although for some fits the difference was as large as 10 ps. Much of this variation is due to the background subtraction. T_0 is very sensitive to the magnitude of this background, and if too little or too much of the background is subtracted, T_0 will appear to be early or late compared to the T_0 of the Br_2 double resonance. Despite these variations, consistent time constants were recorded with reasonably small uncertainty, as the error analysis will show. While the large uncertainty in T_0 does not lead to a corresponding large uncertainty in the time constants, it does mean that we may be missing indications of additional dissociation mechanisms. For example, a short-lived IVR intermediate might show up as the T_0 shifting to later time by a few picoseconds. However, such a shift would not be noticed given the uncertainty in T_0. It is very unlikely, however, that this T_0 uncertainty is hiding important dissociation mechanisms significantly different from the sequential mechanism described in the text. Otherwise, the fits to the delay scans would not have given self-consistent sets of τ_1 and τ_2 values.

Error analysis for each delay scan is done by performing numerical simulations of the entire fitting procedure, similar to the procedures used in Refs. 11 and 47. Synthetic delay scans are generated by sampling at each delay time from a probability distribution with a mean given by the best-fit function to the experimental scan and standard deviation given by the experimental noise. To test for the sensitivity of the time constants to the background-subtraction procedure, the intensity scale factor of the background scan is allowed to vary by more than 20%. The size of the variation in the background scan magnitude is chosen to be large enough to encompass the variations in the background intensity observed in the excitation scans as well as the noise in the background delay scans. The simulated delay scans are fitted, and the time constant(s) are extracted. By this method, at least 50 synthetic delay scans are generated and fitted. The error bars are obtained from the standard deviations (σ) of the set of best-fit time constants extracted from the artificial delay scans. It is important to note that this error-analysis procedure does not account for possible systematic errors introduced in the fitting procedure, especially in the background subtraction. For example, the $Ne_2{}^{79}Br_2$ resonance in the excitation spectra of Fig. 3 is flanked by the $Ne_2{}^{79-81}Br_2$ resonance to the red and a small unknown feature to the blue, both of which may contribute some intensity in the on-resonance delay scan. This contribution would not be accounted for when the pump is detuned to excite only the background.

[1] J. M. Papanikolas, J. R. Gord, N. E. Levinger, D. Ray, V. Vorsa, and W. C. Lineberger, J. Phys. Chem. **95**, 8028 (1991).
[2] A. Sanov and W. C. Lineberger, PhysChemComm **5**, 165 (2002).
[3] W. Sharfin, K. E. Johnson, L. Wharton, and D. H. Levy, J. Chem. Phys. **71**, 1292 (1979).

[4] J. E. Kenny, K. E. Johnson, W. Sharfin, and D. H. Levy, J. Chem. Phys. **72**, 1109 (1980).
[5] A. Rohrbacher, N. Halberstadt, and K. C. Janda, Annu. Rev. Phys. Chem. **51**, 405 (2000).
[6] J. A. Beswick and J. Jortner, Chem. Phys. Lett. **49**, 13 (1977).
[7] G. E. Ewing, J. Chem. Phys. **71**, 3143 (1979).
[8] D. D. Evard, C. R. Bieler, J. I. Cline, N. Sivakumar, and K. C. Janda, J. Chem. Phys. **89**, 2829 (1988).
[9] N. Halberstadt, S. Serna, O. Roncero, and K. C. Janda, J. Chem. Phys. **97**, 341 (1992).
[10] M. L. Burke and W. Klemperer, J. Chem. Phys. **98**, 6642 (1993).
[11] M. A. Taylor, J. M. Pio, W. E. van der Veer, and K. C. Janda, J. Chem. Phys. **132**, 104309 (2010).
[12] K. E. Johnson, W. Sharfin, and D. H. Levy, J. Chem. Phys. **74**, 163 (1981).
[13] W. D. Sands, C. R. Bieler, and K. C. Janda, J. Chem. Phys. **95**, 729 (1991).
[14] S. R. Hair, J. I. Cline, C. R. Bieler, and K. C. Janda, J. Chem. Phys. **90**, 2935 (1989).
[15] C. R. Bieler, D. D. Evard, and K. C. Janda, J. Phys. Chem. **94**, 7452 (1990).
[16] D. S. Boucher, J. P. Darr, D. B. Strasfeld, and R. A. Loomis, J. Phys. Chem. A **112**, 13393 (2008).
[17] B. A. Swartz, D. E. Brinza, C. M. Western, and K. C. Janda, J. Phys. Chem. **88**, 6272 (1984).
[18] J. C. Drobits and M. I. Lester, J. Chem. Phys. **86**, 1662 (1987).
[19] J. I. Cline, B. P. Reid, D. D. Evard, N. Sivakumar, N. Halberstadt, and K. C. Janda, J. Chem. Phys. **89**, 3535 (1988).
[20] M. I. Hernández and N. Halberstadt, J. Chem. Phys. **100**, 7828 (1994).
[21] M. I. Hernández, N. Halberstadt, W. D. Sands, and K. C. Janda, J. Chem. Phys. **113**, 7252 (2000).
[22] J. I. Cline, N. Sivakumar, D. D. Evard, C. R. Bieler, B. P. Reid, N. Halberstadt, S. R. Hair, and K. C. Janda, J. Chem. Phys. **90**, 2605 (1989).
[23] M. Gutmann, D. M. Willberg, and A. H. Zewail, J. Chem. Phys. **97**, 8048 (1992).
[24] P. Villarreal, O. Roncero, and G. Delgado-Barrio, J. Chem. Phys. **101**, 2217 (1994).
[25] M. I. Hernández, A. García-Vela, C. García-Rizo, N. Halberstadt, P. Villarreal, and G. Delgado-Barrio, J. Chem. Phys. **108**, 1989 (1998).
[26] A. García-Vela, J. Chem. Phys. **122**, 014312 (2005).
[27] A. García-Vela, J. Chem. Phys. **122**, 216101 (2005).
[28] A. Valdés, R. Prosmiti, P. Villarreal, and G. Delgado-Barrio, J. Chem. Phys. **122**, 044305 (2005).
[29] O. Roncero, R. P. de Tudela, M. P. de Lara-Castells, R. Prosmiti, G. Delgado-Barrio, and P. Villarreal, Int. J. Quantum Chem. **107**, 2756 (2007).
[30] G. C. Schatz, V. Buch, M. A. Ratner, and R. B. Gerber, J. Chem. Phys. **79**, 1808 (1983).
[31] A. Garcia-Vela, P. Villarreal, and G. Delgado-Barrio, J. Chem. Phys. **92**, 6504 (1990).
[32] P. Villarreal, S. Miret-Artés, O. Roncero, S. Serna, J. Campos-Martínez, and G. Delgado-Barrio, J. Chem. Phys. **93**, 4016 (1990).
[33] F. Le Quéré and S. K. Gray, J. Chem. Phys. **98**, 5396 (1993).
[34] A. Bastida, B. Miguel, J. Zúñiga, A. Requena, N. Halberstadt, and K. C. Janda, J. Chem. Phys. **111**, 4577 (1999).
[35] M. Ceotto and A. García-Vela, J. Chem. Phys. **115**, 2146 (2001).
[36] A. García-Vela, J. Chem. Phys. **116**, 6595 (2002).
[37] B. Miguel, A. Bastidá, J. Zúñiga, A. Requena, and N. Halberstadt, Faraday Discuss. **118**, 257 (2001).
[38] A. García-Vela, P. Villarreal, and G. Delgado-Barrio, J. Chem. Phys. **94**, 7868 (1991).
[39] S. K. Gray, Faraday Discuss. **97**, 143 (1994).
[40] J. Campos-Martínez, M. I. Hernández, O. Roncero, P. Villarreal, and G. Delgado-Barrio, Chem. Phys. Lett. **246**, 197 (1995).
[41] A. García-Vela, J. Rubayo-Soneira, G. Delgado-Barrio, and P. Villarreal, J. Chem. Phys. **104**, 8405 (1996).
[42] A. Bastida, J. Zuñiga, A. Requena, N. Halberstadt, and J. A. Beswick, J. Chem. Phys. **109**, 6320 (1998).
[43] S. F. Alberti, N. Halberstadt, J. A. Beswick, A. Bastida, J. Zúñiga, and A. Requena, J. Chem. Phys. **111**, 239 (1999).
[44] E. Carmona-Novilla, J. Campos-Martínez, M. I. Hernández, O. Roncero, P. Villarreal, and G. Delgado-Barrio, Mol. Phys. **98**, 1783 (2000).
[45] C. Meier and U. Manthe, J. Chem. Phys. **115**, 5477 (2001).
[46] J. A. Cabrera, C. R. Bieler, B. C. Olbricht, W. E. van der Veer, and K. C. Janda, J. Chem. Phys. **123**, 054311 (2005).
[47] J. Cabrera, C. R. Bieler, N. McKinney, W. E. van der Veer, J. M. Pio, K. Janda, and O. Roncero, J. Chem. Phys. **127**, 164309 (2007).
[48] J. M. Pio, W. E. van der Veer, C. R. Bieler, and K. C. Janda, J. Chem. Phys. **128**, 134311 (2008).
[49] The $B \leftarrow X$ and $E \leftarrow B$ transitions of the free Br_2 are assigned using the data from Refs. 69 and 70, respectively.
[50] W. E. van der Veer, Laser Focus World **37**, 141 (2001).
[51] F. Thommen, D. D. Evard, and K. C. Janda, J. Chem. Phys. **82**, 5295 (1985).
[52] A. Rohrbacher, J. Williams, and K. C. Janda, Phys. Chem. Chem. Phys. **1**, 5263 (1999).
[53] D. S. Boucher, D. B. Strasfeld, R. A. Loomis, J. M. Herbert, S. E. Ray, and A. B. McCoy, J. Chem. Phys. **123**, 104312 (2005).
[54] J. P. Darr, R. A. Loomis, and A. B. McCoy, J. Chem. Phys. **122**, 044318 (2005).
[55] J. P. Darr and R. A. Loomis, J. Chem. Phys. **129**, 144306 (2008).
[56] P. P. Chandra and T. A. Stephenson, J. Chem. Phys. **121**, 2985 (2004).
[57] T. A. Stephenson, Y. Hong, and M. I. Lester, J. Chem. Phys. **94**, 4171 (1991).
[58] J. M. Hutchison, R. R. O'Hern, T. A. Stephenson, Y. V. Suleimanov, and A. A. Buchachenko, J. Chem. Phys. **128**, 184311 (2008).
[59] J. I. Cline, D. D. Evard, B. P. Reid, N. Sivakumar, F. Thommen, and K. C. Janda, in *Structure and Dynamics of Weakly Bound Molecular Complexes*, edited by A. Weber (Reidel, Dordrecht, 1987), pp. 533–551.
[60] M. Nejad-Sattari and T. A. Stephenson, J. Chem. Phys. **106**, 5454 (1997).
[61] T. A. Stephenson and N. Halberstadt, J. Chem. Phys. **112**, 2265 (2000).
[62] J. Ogilvie and F. Y. Wang, J. Mol. Struct. **273**, 277 (1992).
[63] A. García-Vela and K. C. Janda, J. Chem. Phys. **124**, 034305 (2006).
[64] A. García-Vela, J. Chem. Phys. **126**, 124306 (2007).
[65] A. García-Vela, J. Chem. Phys. **129**, 094307 (2008).
[66] N. Halberstadt, J. A. Beswick, and K. C. Janda, J. Chem. Phys. **87**, 3966 (1987).
[67] R. F. Barrow and K. K. Yee, J. Chem. Soc., Faraday Trans. 2 **69**, 684 (1973).
[68] A. Burroughs, G. Kerenskaya, and M. C. Heaven, J. Chem. Phys. **115**, 784 (2001).
[69] R. Barrow, T. Clark, J. Coxon, and K. Yee, J. Mol. Spectrosc. **51**, 428 (1974).
[70] T. Ishiwata, A. Tokunaga, T. Shinzawa, and I. Tanaka, Bull. Chem. Soc. Jpn. **57**, 1317 (1984).